The Relationship between the September 2017 Space Weather Event and the Crustal Magnetic Field of Mars

Camella-Rosa Nasr

Department of Astrophysical and Planetary Sciences
Laboratory for Atmospheric and Space Physics
University of Colorado Boulder

Honors Thesis Committee

Dr. Nicholas Schneider, Thesis Advisor
Department of Astrophysical and Planetary Sciences
Laboratory for Atmospheric and Space Physics

Dr. Ann-Marie Madigan, Honors Council Representative
Department of Astrophysical and Planetary Sciences
Joint Institute for Laboratory Astrophysics

Dr. Derek Brown, Thesis Committee Member
Department of Atmospheric and Oceanic Sciences

Defended 6th April 2018

Abstract

In September 2017, the Imaging UltraViolet Spectrograph (IUVS) on the Mars Atmosphere and Volatile Evolution Mission (MAVEN) spacecraft detected a global aurora event that took place as a consequence of an unexpectedly strong blast from the sun. The most widespread of these detected auroras is diffuse aurora, which was confirmed to be global aurora. This global aurora was seen at lower altitudes and has been discovered to be directly related to the detection of highly energetic solar outbursts. These outbursts are typically energetic electrons precipitating downwards (Schneider et al., 2015). I was interested in learning more about the aurora that appeared for the length of the event. I have focused especially on the aurora seen on September 14th, during the declining phase of the aurora event, because it will allow me to determine whether there might be a connection between the observed diffuse aurora event and discrete auroral processes. I have determined the nature of the auroral data that was collected on September 14th, and have used it to draw a conclusion about the relationship between the auroral processes on Mars that took place due to the September 2017 space weather event, and the crustal magnetic field on the surface of Mars. This aurora was "discrete aurora," and it was located in the cusp regions of the crustal magnetic field, where the magnetic field lines have a high probability of being open. The particles that have caused the formation of this aurora are likely to be electrons or low-energy protons.

Contents

List of Tables

List of Figures

Chapter 1

Introduction

Upon MAVEN's detection of aurora that was 25 times brighter than anything MAVEN had ever detected before, I became interested in learning more about the aurora that was seen during the space weather event, especially that which was seen during the declining phase of the aurora event. The nature of the detections will allow for the determination of the nature of the connection between the observed auroral processes and the crustal magnetic field of Mars.

1.1 What is MAVEN?

The Mars Atmosphere and Volatile Evolution mission (MAVEN) launched on November 18, 2013, and has been in orbit around Mars since September 21, 2014. The mission's goal is to explore the interactions of Mars with the Sun, solar wind, and solar energized particles (SEPs), as well as the planet's upper atmosphere and ionosphere. The mission focuses on how the planet lost most of its atmosphere–which is composed of volatile compounds like CO_2, N_2, and H_2O–to space (LASP, 2018). At present, Mars has a very thin atmosphere that is domminated by carbon dioxide. The surface pressure is less that 1% that o Earth. Understanding atmospheric loss will give scientists insight into the history of Mars' atmosphere and climate, liquid water, and planetary habitability (Kramer, 2017).

Research done on MAVEN shows that there is quite a lot of evidence to prove that the escape of gas from the Martian atmosphere to space may have been a significant process. This significant process could have contributed substantially to the change in climate of Mars over time, which was inferred from previous geological and geochemical observations. Other potential processes that could have led to the removal of gas from the atmosphere may possibly include the formation of carbon or other water-bearing minerals in the crust from atmospheric CO_2 and H_2O compounds, as well as the drainage of water from the atmosphere into the crust. Currently, these latter processes appear to be insufficient in magnitude to be able to explain the climate change of Mars. However, the total quantity of the atmosphere that has been lost to space, and the relative importance of the aforementioned processes, is

still a mystery to this day (Jakosky et al., 2015).

MAVEN carries 9 instruments that include: the Imaging UltraViolet Spectrograph (IUVS), the Neutral Gas and Ion Mass Spectrometer (NGIMS), Solar Energetic Particle (SEP). Each of these instruments has its own task when collecting data in order to study the Martian atmosphere (Jakosky et al., 2015). For my project, I used data that was collected by the IUVS machine on the spacecraft.

IUVS is a remote-sensing instrument that measures the ultraviolet (UV) spectra with four observing modes: limb scans near the periapse of the spacecraft's orbit around Mars, planetary mapping at two spectral resolutions, coronal mapping, and stellar occultations. MAVEN plans to use the data collected by IUVS to provide the composition and structure of Mars' upper atmosphere, ionosphere, and corona, as well as the photochemical loss rates for C, N, and O, and the Jeans escape rates for H, D, and He. It will also provide stable-isotope ratios and measure CO_2 photoionization emissions as a proxy for the solar EUV flux (Jakosky et al., 2015). After reaching Mars, the MAVEN spacecraft entered a near-polar orbit with a 75° inclination. At apoapsis, the spacecraft is about 6250 km from the planet, and at periapsis, it is nearly 160 km from the planet. Each orbit lasts for about 4.5 hours. The orbit is not a perfect ellipse, as it precesses around the planet due to the combination of gravitational and atmospheric drag effects, allowing a wide variety of data to be collected. IUVS uses a long, narrow slit ($11° \times 0.06°$) in the telescope focal plane which allows it to define the instrument instantaneous field of view (IFOV) and to provide entrance to the spectrograph. At any instant in time, IUVS uses array detectors to record images which have spectral data in one dimension and spatial variations along the length of the slit in the other dimension. As long as the slit is being displaced in a motion that is perpendicular to its long axis, it can record spectral vs. spatial images, as well as altitude profiles and disk maps (McClintock et al., 2015).

I have looked carefully at the data that was collected at the apoapse of the spacecraft's orbit around the planet (see figure 1.1). I explore this further in the following section of this paper.

Therefore, MAVEN's main goals are to measure the following: the composition and structure of the upper atmosphere and ionosphere today in order to determine the processes responsible for controlling them, the rate of loss of gas and particles from the top of the atmosphere to space, and the properties and characteristics that will allow us to determine the integrated loss to space over the four-billion-year history recorded in the geological record (Jakosky et al., 2015).

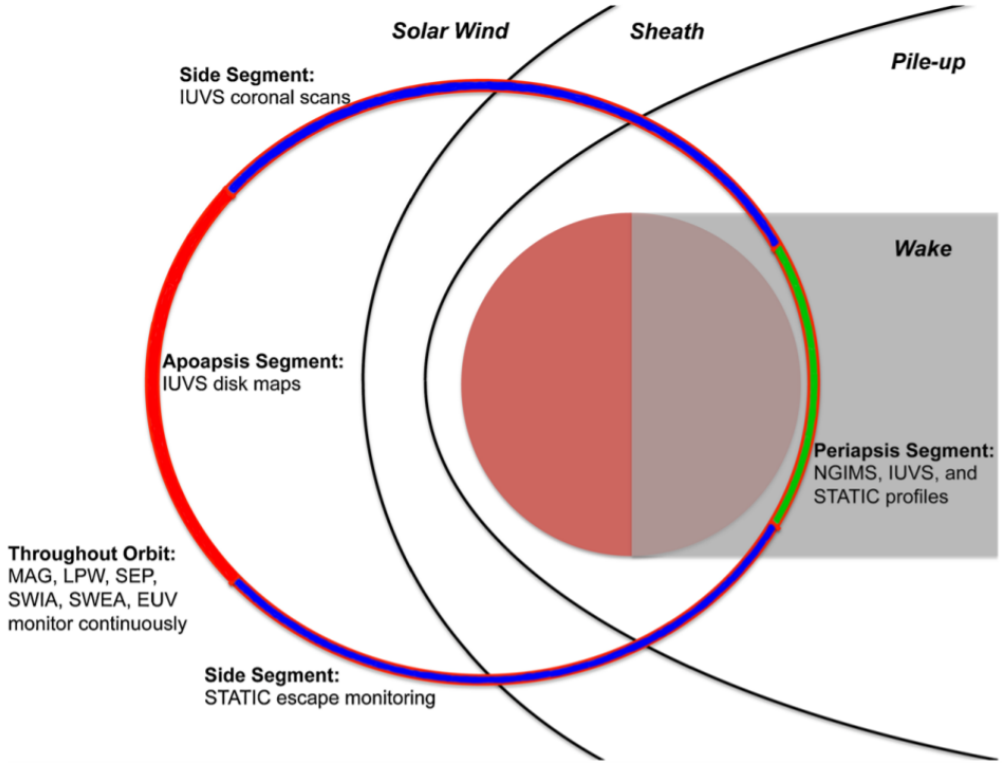

Figure 1.1. Types of data collected by the MAVEN spacecraft while it is in orbit around Mars. The Sun is to the left (figure is from Jakosky et al., 2015).

The data that was used for this project was collected in the highlighted red portion of the orbit in the above figure.

1.2 Three Kinds of Aurora on Mars

It is important to study the auroral emissions in a planet's atmosphere in order to understand the relationship between that planet's atmosphere and its surrounding plasma environment. The collision of solar energetic particles (SEPs) with planetary atmospheres is nearly unavoidable, so auroras are phenomena that are quite widespread among the planets in our Solar System. Auroras have been detected at all planets with substantial atmospheres, like the Jovian planets, as well as at some moons with atmospheres. These planetary auroras are usually discrete, if they are detected at planets or moons with intrinsic magnetic fields. At planets or moons with no intrinsic magnetic fields, the auroras that have been detected have been diffuse auroras (Schneider et al., 2015). In our Solar System, auroral emissions in planetary atmospheres typically result from the impact of energized particles other than photoelectrons. Auroral activity has been found on all four giant planets (Jupiter, Saturn, Uranus, and Neptune) possessing a magnetic field, but they have also been found on planets (like Venus) with no magnetic field (Bertaux et al., 2005).

On August 11, 2004, the Spectroscopy for Investigation of Characteristics of the Atmosphere of Mars (SPICAM) UV instrument on board the Mars Express made the first observation of auroral-type emissions on the nightside of Mars (Leblanc et al., 2006).

The IUVS instrument captures the planet and atmosphere's reflectance and emission spectra in the far-ultraviolet (FUV: 110 to 190 nm) and mid-ultraviolet (MUV: 180 to 340 nm) regions, because those two are ideal for recording well-known atmospheric emissions from CO_2, as well as its dissociation and ionization products. Three types of MUV spectra have been observed by IUVS at Mars. The largest telltale sign of an aurora is the presence of dayside spectroscopic features in selected nightside spectra. Some of these features include the CO Cameron bands, the $CO_2{}^+$ and ultraviolet doublet (UVD), and oxygen, which peaks at around 297 nm. It is important to note that all emissions are ultimately due to the dissociation and ionization of CO_2, which is the most abundant gas in the atmosphere of Mars. In the absence of sunlight, so on the night side of the planet, emissions can only be produced as a result of energetic particle excitation. No auroral emission has been detected in the FUV wavelength range as of right now, but the search for weak spectral features is still ongoing. The auroral emissions that have been detected so far are about 100 times weaker than their dayglow counterparts (emissions that have been seen on the dayside of the planet) (Schneider et al., 2015).

Mars no longer has an intrinsic global magnetic field, but remnants of such a field still exist trapped in certain areas of the crust, thereby allowing scientists to expect that aurora would occur near areas where the crustal magnetic field lines are open. These expectations were confirmed when three kinds of aurora were detected on Mars: diffuse aurora, discrete aurora, and proton aurora.

1.2.1 Diffuse Aurora

This kind of aurora is the most widespread, and it was discovered at low altitudes, coincidentally with the detection of highly energetic solar outbursts. During these outbursts, energetic electrons precipitate downwards to great depths in the atmosphere, to an average altitude of 70 km, depositing their energy below the homopause (Connour et al., 2017). The homopause is the level of the atmosphere below which its constituent molecules are well mixed (Weisstein, 2007).

This type of aurora is neither restricted in location nor linked to the Martian magnetic field (Ritter et al., 2018). SPICAM may not have been sensitive enough to detect diffuse aurora, but IUVS was able to make those detections. Mars' diffuse aurora has a lot in common with auroras that have been seen on Venus and some moons of Jovian planets. Diffuse auroras are not surprising at Venus, which lacks a global magnetic field and any crustal fields (Schneider et al., 2015). This kind of aurora is also characterized by its distribution at an altitude lower than the discrete aurora. To reiterate, diffuse aurora are attributed to solar energetic particles (SEPs), specifically electrons that are accelerated to energies of around 100 keV at the Sun and heliospheric shock fronts (Gérard et al., 2017).

1.2.2 Discrete Aurora

Discrete aurora was first observed as spatially confined auroral features in a limb scan by SPICAM. Subsequently, other observations of the discrete aurora were reported, and they revealed that these features are linked to the topology of the crustal magnetic field of Mars (Ritter et al., 2018a). Discrete auroras have typically been detected by IUVS in the Southern Hemisphere of Mars. And similarly to diffuse auroras, discrete auroras are created by the precipitation of energetic electrons. However, unlike diffuse auroras which have been seen to be global, discrete auroras are typically confined to the crustal magnetic field and have only been detected to be sustained for a few minutes. Some of the additional differences between these two kinds of auroras include the spectroscopic signatures that differ significantly between the two, indicating that different physical processes are involved with excitation and quenching of these auroras (Schneider et al., 2018).

Studying discrete aurora more closely has caused them to be attributed to particles accelerated to energies that are typically less than 1 keV by magnetic field reconfiguration at Mars, and have been primarily observed at altitudes around 140 km (Gérard et al., 2015; Brain et al., 2006). Discrete auroras provide concrete evidence of particle precipitation into the Martian night side atmosphere in localized regions, and the likely effects of more global precipitation of charged particles during both quiet and solar storm periods have also been considered (Schneider et al., 2018).

It is theorized that the discrete aurora that is being observed on Mars has a similar source to terrestrial discrete aurora. At the moment, it is being suggested that where there are crustal fields, there are resulting complex rotating interactions with the variable solar wind that allows for particle acceleration to take place (Ritter et al., 2018a). This explains why discrete aurora is likely to be detected in boundaries, or cusps, of crustal magnetization regions on the surface of Mars.

It is also important to make the following distinction between the aforementioned two kinds of aurora: Mars discrete aurora are caused by electrons moving on or near closed field lines associated with crustal fields in the southern hemisphere of the planet; whereas Mars diffuse aurora must be a new process, with energetic solar electrons directly penetrating the atmosphere. For this new process to take place, electrons typically travel along open field lines (Schneider et al., 2015).

1.2.3 Proton Aurora

IUVS discovered a third form called proton aurora occurring on Mars' dayside, caused by penetrating protons from the solar wind (Deighan et al., 2018; Halekas et al., 2017). The MAVEN/IUVS detection of proton aurora prompted a search in the Mars Express SPICAM archive (Ritter et al., 2018b), finding six events and confirming the existence of the phenomenon (Schneider et al., 2018).

The proton aurora is seen as intensity increases in the Lyman-α emissions at altitudes between 120 and 150 km. It has been observed with IUVS and SPICAM in 6 out of 143 observation

sequences and is related to the arrival of coronal mass ejections or co-rotating interaction regions at Mars. *Ritter et al., 2018b* have used Monte Carlo modeling to reproduce the intensity enhancement at these altitudes. This modeling has revealed how the Lyman-α line profile and intensity change in the presence of an induced magnetic field. And even though the Lyman-α emission is the strongest emission to be seen in proton aurora, the aurora also appears to manifest in the visible (Balmer series), at the peak of the H-β line at 486.1 nm (Ritter et al., 2018b).

Detection of these aurora is usually characterized by a 50% increase in peak emission, and these aurora have only been detected to last up to a few hours. The energetic hydrogen atoms from solar wind activity enter Mars' thermosphere where they are repeatedly excited through elastic collisions, electron stripping, and charge exchange reactions, which leads to them emitting Lyman-α photons when they are neutral (Connour et al., 2017).

For the sake of this project, I have chosen to focus primarily on the diffuse and discrete auroral processes on Mars.

1.3 Comparing Mars Aurora to Earth Aurora

At least three different kinds of aurora have been seen on Earth. These have been studied by combining observations of both the precipitating particles and the emitted photon radiation. On Earth, the most well-known and brightest aurora is discrete aurora. Typically, it is spatially confined within the "auroral ovals" that are surrounding Earth's magnetic poles. This type of aurora is powered by the acceleration of precipitating particles due to some sort of combination of parallel electric fields and plasma waves.

A second type of aurora can occur near the equator of the auroral zones and is caused by particles locked deeper in Earth's magnetic field. This second kind of aurora is named "diffuse aurora" or "drizzle" because it occurs over much wider spatial ranges, and it usually lacks in any noticeable patterns or spatial features. It also differs from discrete aurora in that it results from particles scattered into Earth's atmosphere without acceleration.

A third type of aurora occurs near the poles of the auroral ovals, from particles like solar wind electrons that precipitate into the atmosphere without local acceleration. This third type of aurora could also be labeled as diffuse, and it is called "polar rain aurora," simply to distinguish it from the second kind of aurora that was mentioned earlier.

On Earth, both forms of diffuse aurora are fainter than discrete auroras, which is a resultant of the lower particle flux and energy that cause them. In all three cases, these terrestrial auroras are confined to the polar regions with an emission peak in the upper atmosphere or thermosphere, and they are never seen as a global phenomenon (Schneider et al., 2015).

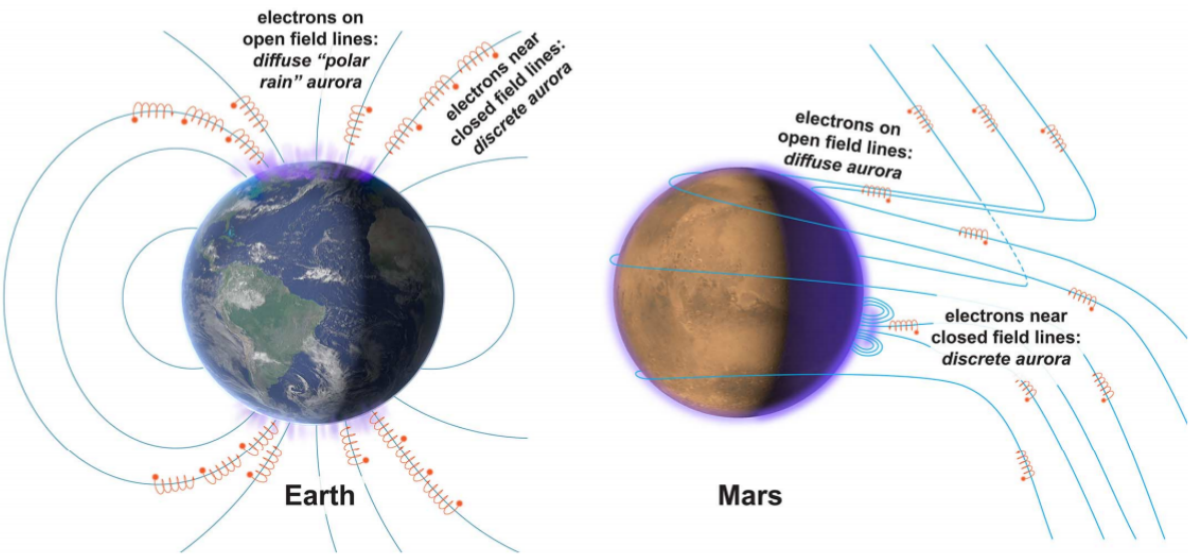

Figure 1.2. Comparison of the magnetic field lines of Earth and Mars (image is from Schneider et al., 2015).

Figure 1.2 shows that Earth still has its own magnetic dynamo, but Mars does not because its atmosphere was stripped by solar wind and its core has cooled down. The most prominent magnetic field lines on Mars are those that have been trapped in the crust for millions of years. These differences in the magnetic field lines explain the differences in diffuse and discrete aurora between Earth and Mars.

Since the detection of diffuse aurora by IUVS, clearer comparisons between Mars auroral phenomena and Earth auroral phenomena can be made, despite the very different natures of their magnetic field line configurations. See figure 1.2.

Diffuse auroral phenomena vary vastly between the two planets. Earth has two types of diffuse aurora, one of which ("drizzle" aurora) occurs very deep within the magnetosphere. Since Mars has a negligible magnetosphere, terrestrial "drizzle" aurora does not have a counterpart on Mars. The other kind of terrestrial diffuse aurora, or "polar rain" aurora, does seem to be a product of electrons that have been excited at the Sun, and not on the surface of the planet, which is a circumstance that seems to be the source of Mars diffuse aurora as well. On Earth, these electrons can collide directly with open field lines near the poles of the planet, and on Mars, they strike the atmosphere far from closed crustal magnetic field lines. This explains why diffuse aurora on Earth is limited to the poles (Schneider et al., 2015).

Mars' field lines, which are open or draped, allow SEPs to penetrate the atmosphere during solar storms. These particles, which have been observed to be 100 to 1000 times more energetic than those causing discrete auroras, reach much lower altitudes in the atmosphere, which explains why diffuse auroras are seen to be lower in the atmosphere. Open and draped field lines often cover most of Mars, though the locations change. The nature of the crustal magnetic field of Mars will be expanded on in Section 3.2.3 of this paper.

Mars has the ability to distort the solar wind magnetic field, which allows for diffuse auroras to occur potentially anywhere and everywhere, all over the planet. This is what makes Mars diffuse aurora more similar to aurora that has been seen on Venus and on the moons of Jovian planets (Schneider et al., 2015).

All in all, discrete auroras occur at Earth in the auroral ovals along the edges of closed field lines, where there are interactions between Earth's magnetic field and the solar wind that lead to the acceleration of particle from the magnetosphere until they reach sufficient energies to cause auroras. Similar interactions probably occur at Mars to cause discrete auroras. Earth's auroral ovals and Mars' discrete auroral patches probably originate analogously, despite their different appearances (Schneider et al., 2015).

1.4 Spectroscopy of CO Cameron Bands in the Martian Atmosphere

Previous studies have shown that the electron impact on CO is the major source mechanism of Cameron bands, followed by electron and photon impact dissociation of CO_2 (Bhardwaj and Jain, 2013). The CO Cameron bands typically range from 170 to 270 nm. These bands, as well as the $CO_2{}^+$ ultraviolet doublet (range: 298 and 299 nm), emissions have been observed on the Mars dayside by the SPICAM instrument in the limb viewing mode. These ultraviolet emissions ultimately arise from the excitation of the neutral atmosphere by solar extreme ultraviolet radiation (Stiepen et al., 2015).

IUVS records a limited MUV spectral range (195-220 nm) in order to spectrally distinguish two important molecular emissions observed on Mars' nightside: CO Cameron bands observed in aurora and nitric oxide (NO) nightglow emissions. The spectra are fitted against templates for these two emissions using multiple linear regression (Schneider et al., 2018). CO Cameron bands are one of the hallmarks of auroral observations on Mars.

I have studied the spectra of observations made during the September 2017 Space Weather event in order to make sure that the brightest detections are, in fact, auroral observations. If a data spectrum matches the CO Cameron band template, then I can confirm that the detections are real discrete auroral detections.

1.5 Nitric Oxide Nightglow

The term "Nightglow" refers to a phenomenon in which a planet's sky faintly glows, even without external light (usually from the Sun). On Mars, this is the result of nitric oxide emissions. Nitric oxide (NO) UV nightglow comes from the de-excitation of NO molecules, which result from radiative recombination. On the dayside thermosphere of Mars, solar extreme ultraviolet radiation causes the photodissociation of CO_2 and N_2 molecules. Oxygen and nitrogen atoms are carried by the day-to-night hemispheric transport, which are at most

times high-altitude winds. They usually end up descending in the nightside mesosphere in the winter hemisphere, where they can radiatively recombine to form NO (Howell, 2017; Stiepen et al., 2017; Schneider et al., 2018).

The image below (figure 1.3) shows the spectrum templates for CO Cameron band and NO emission. Peaks for CO Cameron bands are typically more broad, and allow for an easy distinction to be made between the two features. In addition, CO Cameron bands have a relative brightness that is about 20 times higher than that of NO emissions.

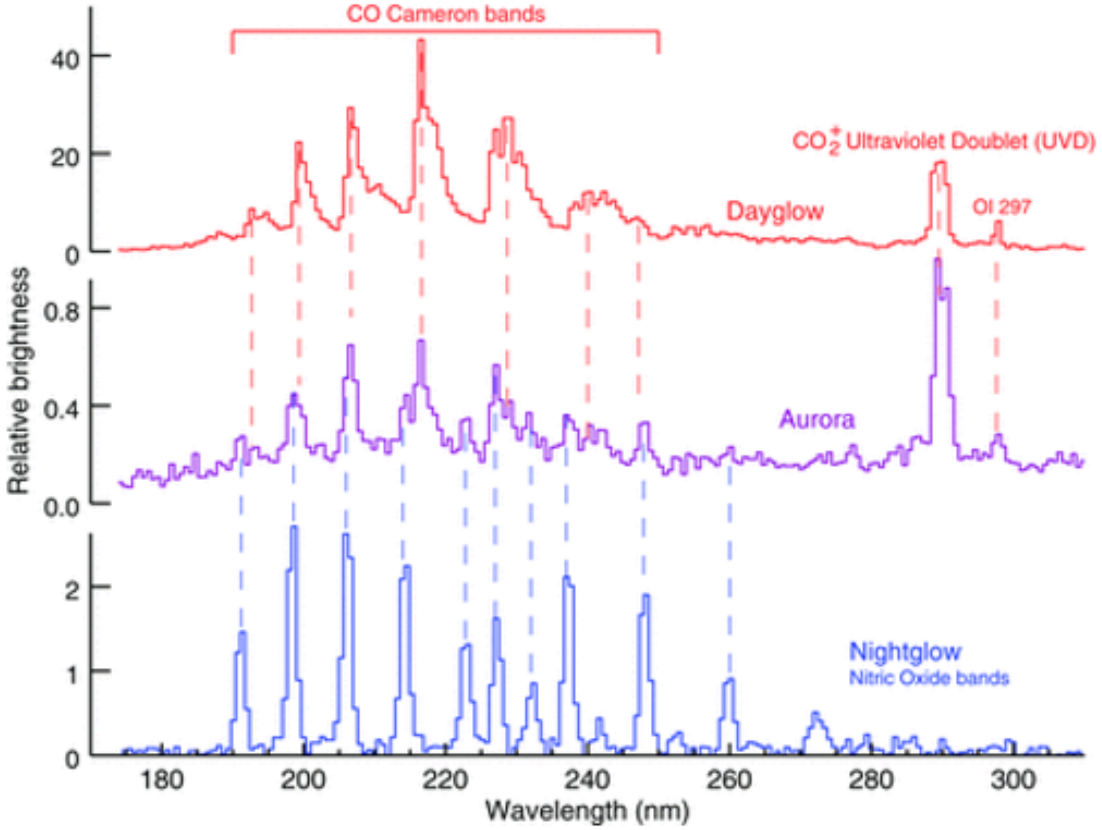

Figure 1.3. Spectral templates for detected emissions in the atmosphere of Mars (image is from Connour et al., 2017).

The data collected by MAVEN is turned into spectra that can be associated with individual pixels. I have added groups of such pixels together in order to compare their spectra to spectral templates for CO Cameron band emission, nitric oxide nightglow, or broadband features associated with cosmic rays or stray light occurring within the instrument. NO emissions were seen in many orbits during the September 2017 Space Weather event.

Chapter 2

Timeline of the September 2017 Space Weather Event

In September 2017, the Imaging UltraViolet Spectrograph (IUVS) on the MAVEN spacecraft observed global aurora on Mars caused by a surprisingly strong solar energetic particle event. The event produced radiation levels on the surface more than double any previously measured by the Curiosity rover's Radiation Assessment Detector, or RAD, since that mission's landing in 2012. The high readings lasted more than two days. The strangest part is that the solar energetic particle event occurred during what is usually a quiet period in the Sun's 11-year sunspot and storm-activity cycle (NASA, 2017).

This event was big enough to be detected at Earth too, even though Earth was on the opposite side of the Sun from Mars. Widespread "diffuse aurora" have previously been detected on Mars through more limited observations (Schneider et al., 2015), but recent observations established complete coverage of the observable portion of Mars' nightside. The aurora was global due to Mars' lack of a global magnetic field, which allowed energetic electrons from the Sun to directly precipitate into the atmosphere. On September 11, IUVS detected aurora more than 25 times brighter than any prior IUVS observation, with a high signal-to-noise ratio (SNR) detections of aurora at the limb and against the disk of the planet. Fainter auroral emission was seen around the nightside limb over 13 orbits spanning nearly 3 days. See figure 2.1.

On September 14, during the declining phase of the event, faint linear features and patches were detected by the spacecraft, which were higher than the noise floor, with a similar spatial distribution to "discrete aurora" patches observed on Mars by the SPICAM instrument on the Mars Express spacecraft (Bertaux et al., 2015). On this day, MAVEN was in its 5738th orbit. This orbit was of special interest to me, and I explore it in detail later in this paper.

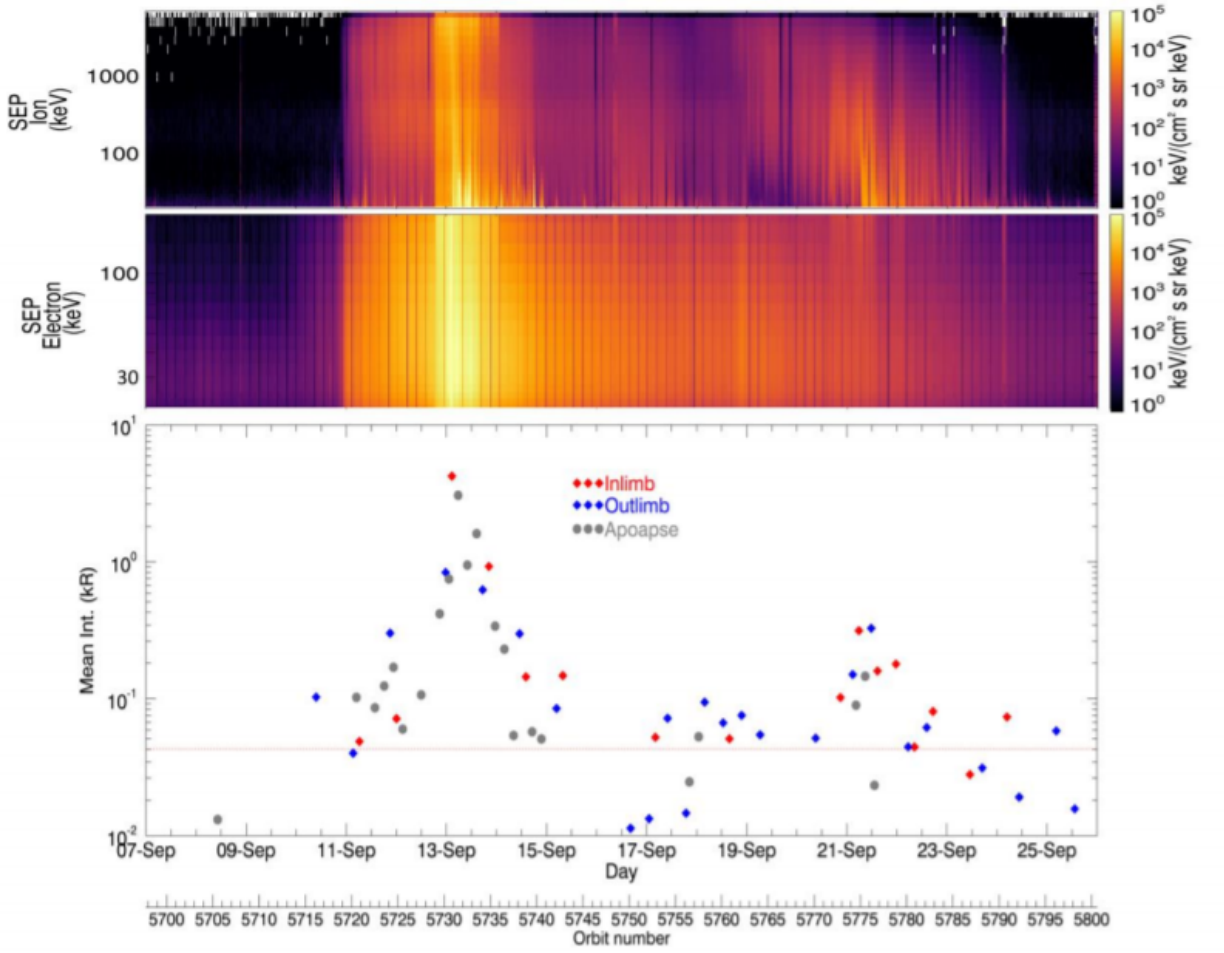

Figure 2.1. Timeline of the September 2017 Space Weather Event (image is from Schneider et al., 2018).

The scatterplot at the bottom of the image above (figure 2.1) shows auroral emission from CO Cameron bands in kiloRayleighs (unit of intensity or brightness). The grey circles show brightnesses in the limb region averaged over 50-100 km extracted from apoapse images. The red and blue diamonds show the brightness average of the same altitude range in limb scans across the emitting layer obtained about an hour before and after the apoapse images. The limb scans focused roughly on the center of the disk seen in the apoapse images. The peak in mean intensity over September 13 represents the brightest aurora that was detected during the event. The spectra on top of the timeline show SEP measurements that were made thousands of kilometers away from the aurora themselves, so a perfect correlation would be unexpected. On its own, the timeline does not identify a unique correlation with either SEP electrons or protons, which is why a separate hunt for the kind of SEPs that is causing this aurora is required (Schneider et al., 2018).

Chapter 3

Observations from the September 2017 Space Weather Event

Peaks in intensity were seen over an extended period from September 7th to September 26th. Figure 2.1 shows the spectrum and altitude profiles of the emission obtained from inlimb observations obtained during orbit 5731 near the peak of the space weather event. The timeline in Figure 2.1 also shows that there are three distinct peaks, which indicate three distinct events: September 11-14, September 17-18, and September 20-21. The first peak is more than ten times brighter than the other two peaks. The primary auroral brightening during the first event correlates well with either SEP electrons or protons, but the second event has no corresponding rise in either SEP electrons or protons, which means that it does not perfectly correlate with what we expect. The third auroral event corresponds better with SEP protons (Schneider et al., 2018).

I have looked more closely at multiple orbits in the first aurora event (Sep 11-14). Orbits 5731 (Sep 13) and 5738 (Sep 14) belong to the first aurora event and I found them to be the most interesting. I have also analyzed other orbits like orbits 5725 (Sep 12), 5731 (Sep 13), 5737 (Sep 14).

For the purpose of the project, I have studied the data collected while the spacecraft was in the apoapse mode, in order to distinguish what kind of aurora was seen in the brightest and most interesting orbits. In addition, I have tried to narrow down what kind of SEPs are the cause of the auroras during this event by studying the gyroradii of corresponding energies that were detected by IUVS.

3.1 Orbit 5731: Brightest Global Aurora

The global aurora was triggered by a space weather event observed by many instruments on board the spacecraft. When a solar storm hits the Martian atmosphere, it can trigger auroras that light up the entire planet in at the UV end of the spectrum because of Mars' lack of a strong global magnetic field. The recent solar storm was so intense that it caused

Mars to glow in a way that it had never done before. SEPs can also be absorbed by the upper atmosphere, which causes particles in the atmosphere to increase in temperature and volume (NASA, 2017). The peak of this event was during Orbit 5731. See figure 3.1.

Since the IUVS slit can only span 11 degrees at a time, only a narrow swath across the planet can be recorded. The complete image can be constructed by taking into account the spacecraft's orbital motion about the planet, which allows for several image swaths to be taken sequentially while the spacecraft is inertially pointed. It is important to note that the each image takes about 70 minutes to be created, and during this time, the imaging and viewing geometry change, so all the swath images below cannot be considered to be snapshots that were taken at a single location and moment in time (Schneider et al., 2018).

The purple-to-white brightness scale in the images below display the brightness(of range 0–2.5 kiloRayleighs) of emission matching the template for CO Cameron bands excited by particle precipitation. IUVS has scanned its slit across Mars in six swaths from left to right, while the spacecraft traveled around Mars from top to bottom (Schneider et al., 2018).

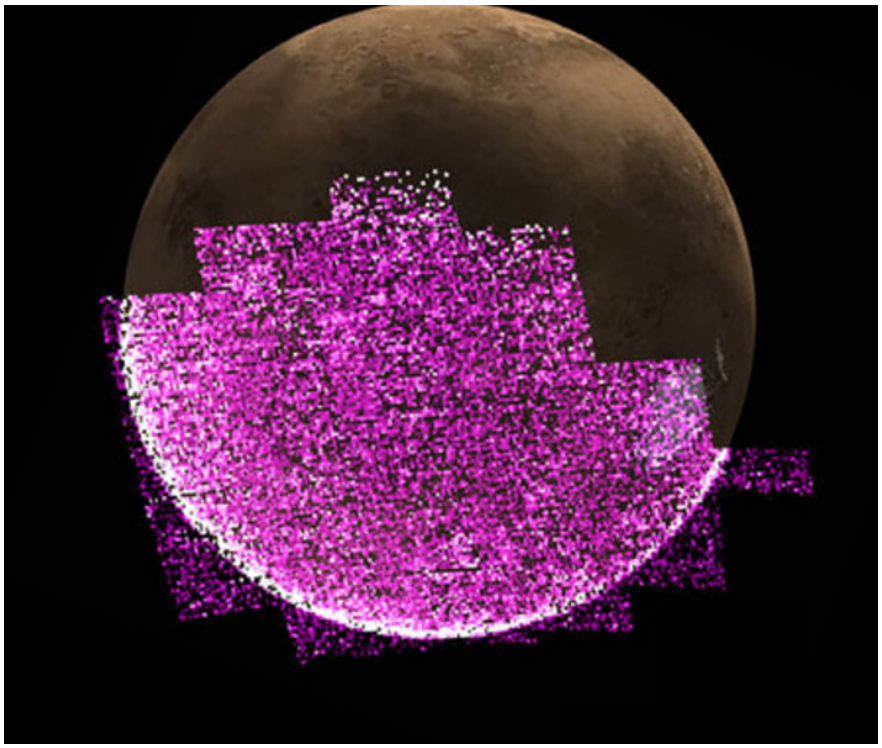

Figure 3.1. Orbit 5731 (taken from Schneider et al., 2018).

The above image (figure 3.1) was taken on 13 Sep 2017 at 05:34 UTC. (Schneider et al., 2018).

Orbit 5731 can easily be distinguished as the orbit with the brightest auroral emission. See figures 3.2 below.

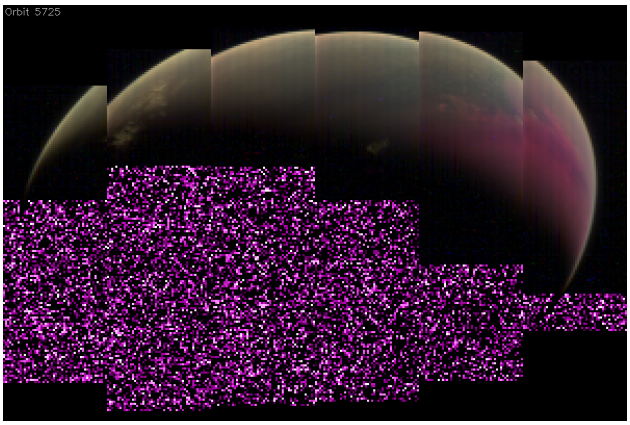

(a) CO Cameron band swath image for orbit 5725

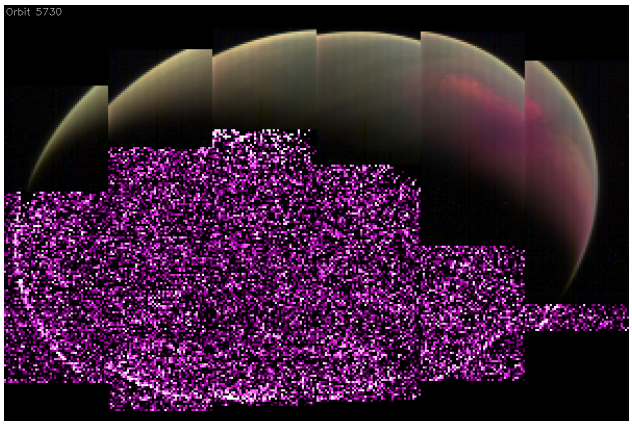

(b) CO Cameron band swath image for orbit 5730

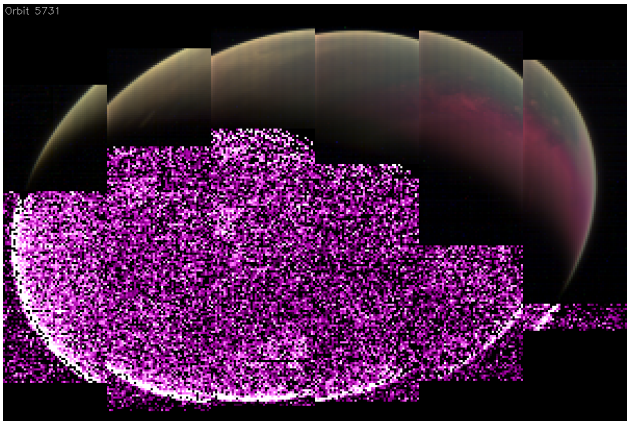

(c) CO Cameron band swath image for orbit 5731

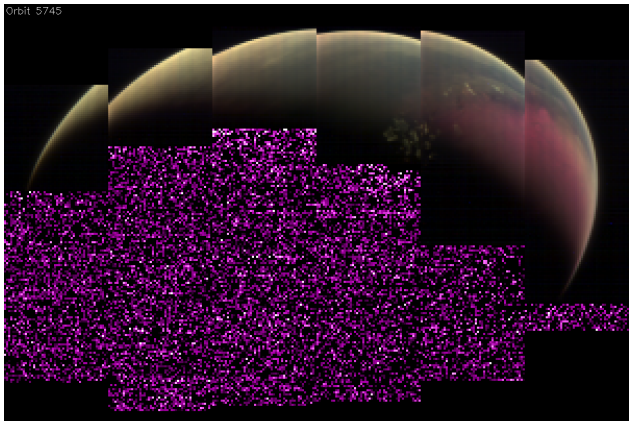

(d) CO Cameron band swath image for orbit 5745

Figure 3.2. Evolution of CO Cameron band swath images for orbits during the aurora event.

In the series of images above (see figure 3.2), orbit 5725 is the first orbit of the event. Orbit 5730 shows bright global aurora, but it is not as bright as the following orbit. Orbit 5731 is easily distinguishable as the one with the brightest global aurora. Orbit 5745 is the last orbit of the event. Auroral detections seem to be very faint for this orbit, which is exactly as expected.

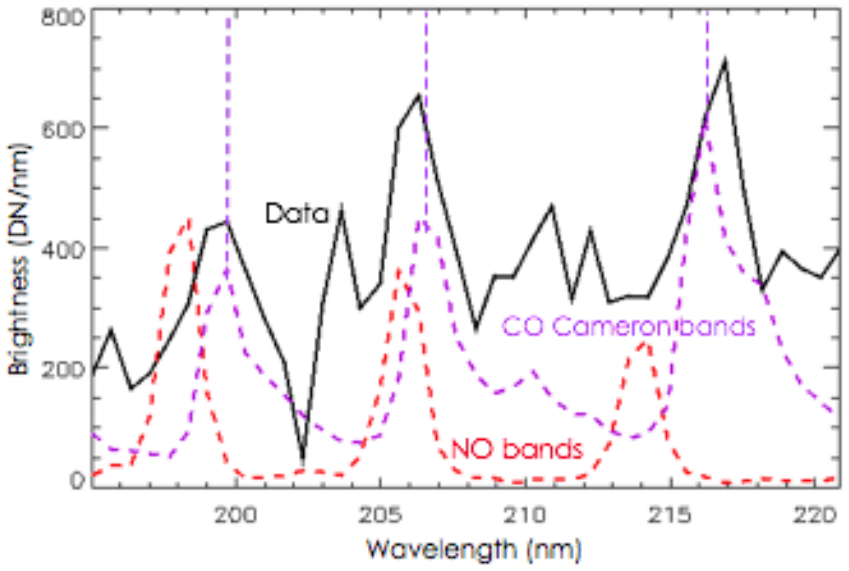

Figure 3.3. The spectrum of a bright area on the disk of the planet during Orbit 5731.

In Figure 3.3, the dotted purple template is that of CO Cameron bands, and the dotted red template is that of NO emission. The solid black line corresponds to the data collected by IUVS. The image shows that the data peaks in the areas where the CO Cameron bands do, which means that it is real auroral data. In addition, since the solid black line peaks at intensities higher than those of the template, it means that the data that was collected was much brighter than previously detected. The locations of the pixels that were co-added together to form this spectrum is in Appendix Table A.1.

3.2 Orbit 5738: Anomalous Auroral Features

During the declining phase of the event, faint linear features and patches (see figure 3.4) were detected by the spacecraft, which had intensities higher than the noise floor. The detected aurora from Orbit 5738, which was limited to a few geographical regions, was seen to only fall in the cusp regions of the crustal magnetic field where the magnetic field lines are pointing radially outwards. After studying the localized auroral emissions on September 14, during Orbit 5738, I can conclude that it is actually discrete aurora, which typically has a very similar spatial distribution, and follows the CO Cameron band template.

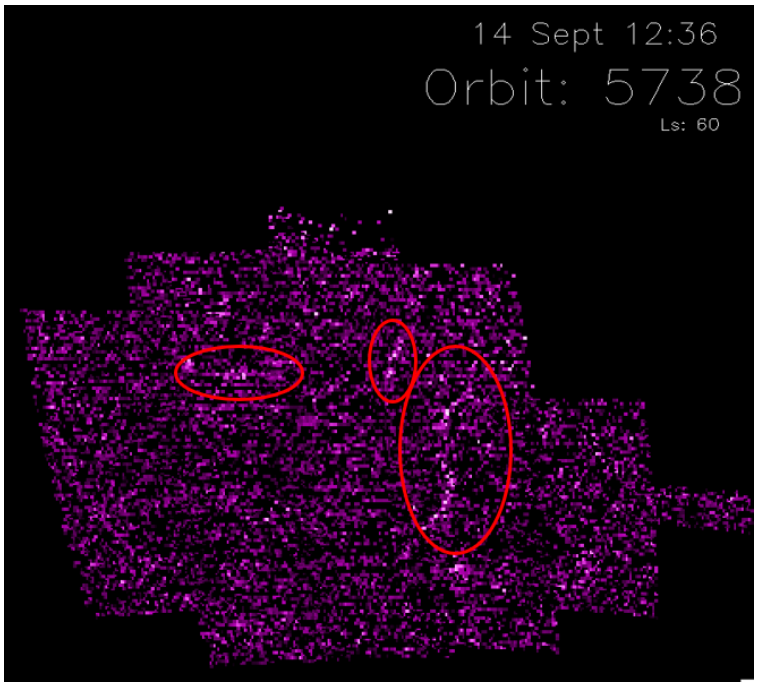

Figure 3.4. The intensity pixels as seen on Sep 14, when the global aurora event had started waning.

The image above (see figure 3.4) shows the very interesting patches of bright pixels that were studied below. The swaths in the image have been altered slightly so that they can appear to follow the spherical nature of the planet.

Meanwhile, the swath image below (see figure 3.5) gives a clear picture of what the patches look like, as well as where they fall on the disk of the planet. The data was collected as the scan mirror of IUVS traveled in one direction and the spacecraft itself traveled in a direction perpendicular to it. Some patches represent real aurora, while others do not.

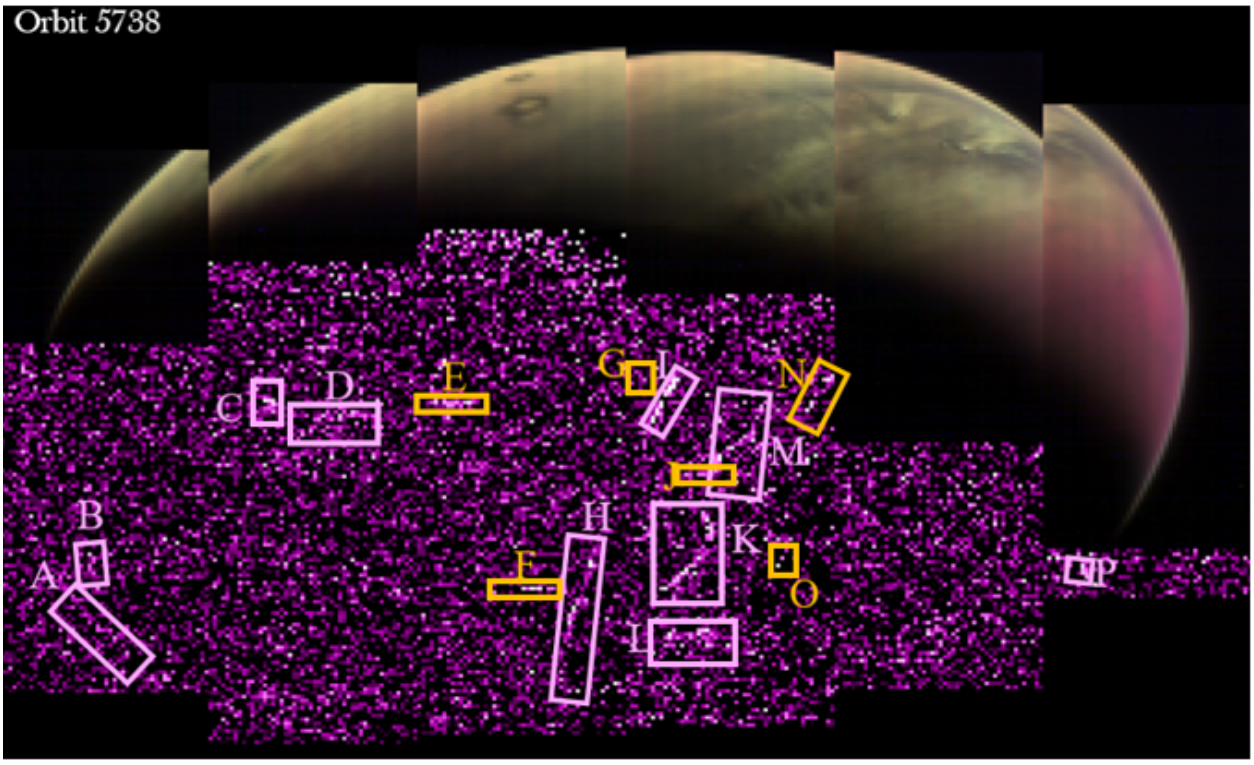

Figure 3.5. The swath image that shows the intensity pixels of the data collected. The areas highlighted in light purple represent real auroral detections, while the areas highlighted in orange represent non-real auroral detections.

3.2.1 Real Auroral Detections vs. Non-Real Auroral Detections

As I have previously mentioned, in order to determine whether the linear features and patches in Orbit 5738 are real, I have studied the spectra of the intensity pixels. If the spectra of the data peak in the exact locations of the three peaks of the CO Cameron band template, then they are considered to be real data, and they would therefore represent real auroral emissions (light purple areas: A, B, C, D, H, I, K, L, M, and P) . If the spectra do not follow the CO Cameron band template, then they are not considered to be real auroral emissions (orange areas: E, F, G, J, O, and N). It is also worth noting that the bright patch of light at the top of the third swath is not real aurora and is simply solar straylight. See figures 3.6 and 3.7. A more intricately-labeled image of orbit 5738 is included in the Appendix section of the paper (see figure A.1).

- Examples of Real Auroral Detections:

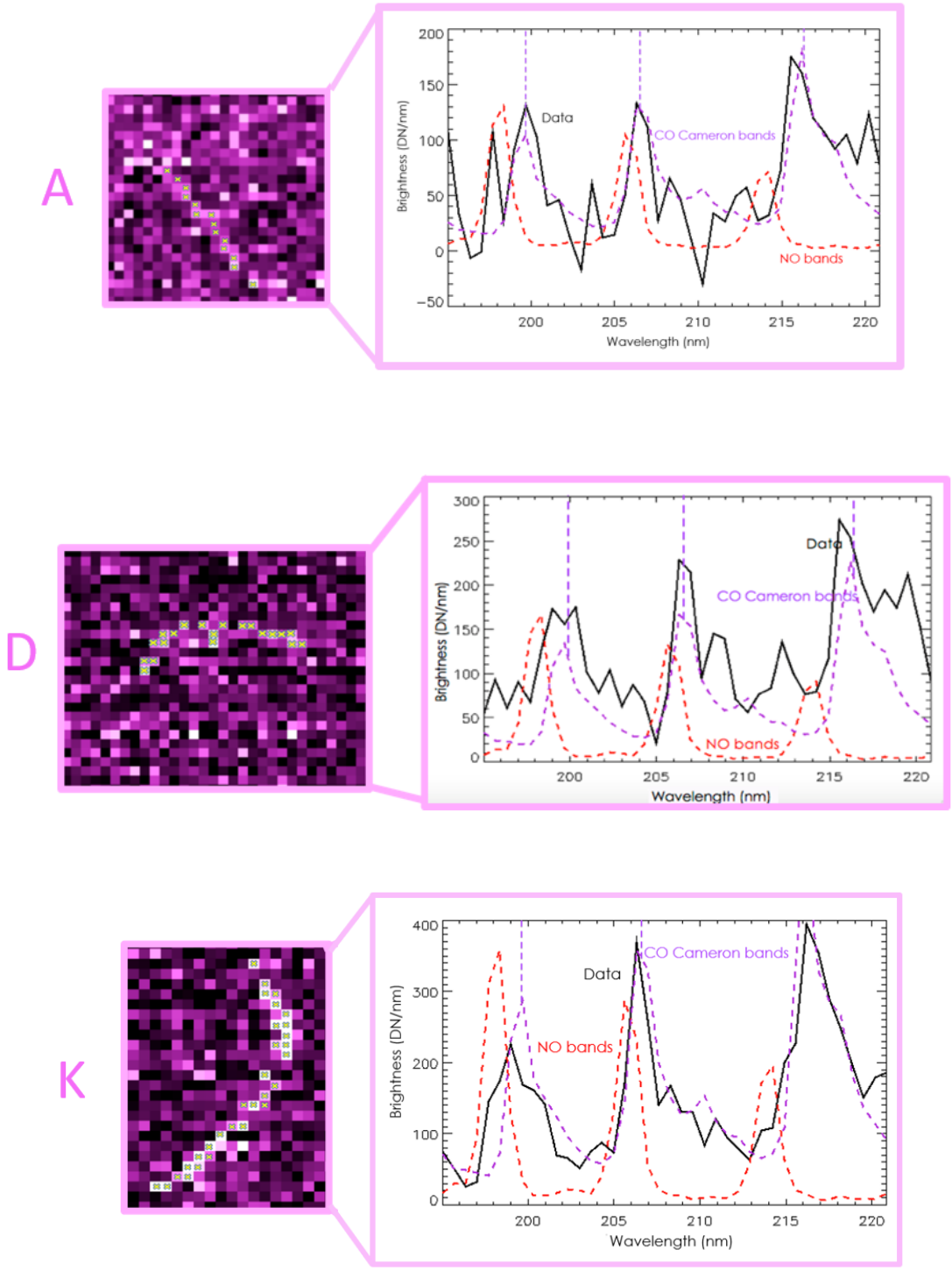

Figure 3.6. Intensity plots of pixels in features A, D, and K.

These plots show that the data matches the CO Cameron band template (dotted purple), since it peaks in the three locations where the template peaks. This allows us to conclude

that the aurora detected here was real. The pixels marked with an 'x' are those that were co-added together to give the spectra to the right.

- Example of Non-Real Auroral Detections:

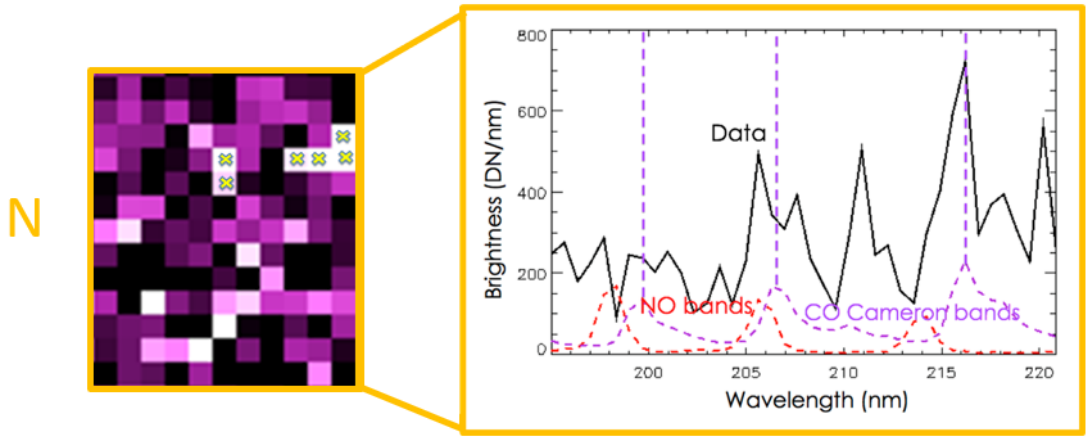

Figure 3.7. Intensity plot of pixels in feature N.

In this case, the data do not match the Cameron band template, so we can say that the observed signal in this area does not represent any auroral features, and is therefore not real.

The locations of the pixels that I used to create these spectrum plots are included in Tables A.2, A.3, A.4, and A.5 in the Appendix.

Finally, since the real auroral features seen in orbit 5738 follow the CO Cameron band template, I have concluded that they can be identified as discrete aurora.

3.2.2 Relationship to the Crustal Magnetic Field

While Mars is known for lacking a strong, global magnetic field, it possesses traces of a crustal magnetic field along certain areas of its surface. In the outer 40 km of the lithosphere of the planet lie rocks that have been magnetized due to Mars' once-strong global dipole field. These rocks allow for a crustal magnetic field to persist along the surface of Mars. The real anomalous aurora features that have been detected on September 14 do seem to be discrete aurora, and they are limited to regions of the crustal magnetic field where the field lines are likely to be more vertical and open to solar wind interactions. Those regions are concentrated in Mars' southern hemisphere centered on 180 degrees east longitude.

I have projected the location of the real and non-real features from orbit 5738 on the crustal magnetic field map that corresponds to this orbit. The map in the background is from Brain et al., 2007. See figure 3.8.

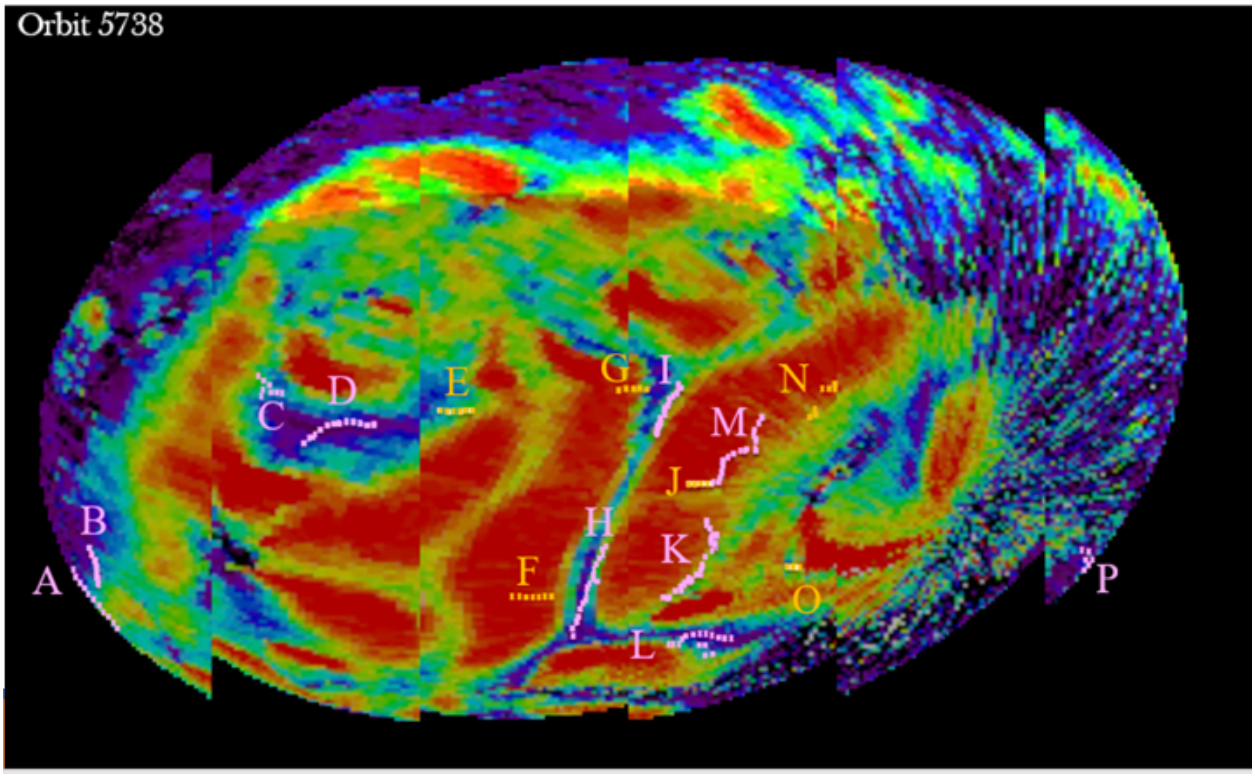

Figure 3.8. Anomalous auroral features overlaid on a crustal magnetic field map.

The image (see figure 3.8) allows us to see that the real auroral detections are in the green and blue areas of the map where the magnetic field lines are open. Any detections that were made in the red areas of the map were not real aurora, since we would not expect to find aurora in areas where the magnetic field lines are closed. Therefore, the locations of the auroral features with respect to the crustal magnetic field match the expectations of whether or not they are real.

In Figure 3.8, the magnetic field map takes into consideration the actual location of the spacecraft with respect to the planet, where the slit is pointing, Mars' rotation, and spacecraft motion. The green areas on the magnetic field map represent areas where the magnetic field lines have a very high probability of being open. The blue areas represent areas where the magnetic field lines are likely to be open 50% of the time and closed the other 50% of the time. Finally, red areas are where the field lines have a high probability of being closed, so they would not allow for the formation of discrete aurora.

Hence, the crustal magnetic field of Mars had a direct influence on faint auroral emissions during the declining phase of the event.

3.2.3 Current State of the Magnetic Field of Mars

Martian crustal magnetic fields, which are much weaker than global dipole fields are strong enough to stand off shocked solar wind to 1000 km altitudes or higher, which protects localized

regions of the atmosphere from solar wind. In some locations, particles from the solar wind plasma can descend directly to the lower ionosphere along open magnetic field lines. These locations are called magnetic cusps, and they are analogous to those found at Earth's poles (Brain et al., 2006). The real auroral detections that were seen in Orbit 5738 were seen along these cusps.

Magnetic field lines at Mars allow for both energy inflow and ion escape. So any local variations in magnetic field topology would directly affect the interaction between the solar wind and the Martian ionosphere. Because Mars lacks a global dynamo, the solar wind directly interacts with the planet's ionosphere. The solar wind carries the interplanetary magnetic field (IMF), which drapes around the planet, and forms an induced magnetosphere similar to those that are found at other unmagnetized bodies in the solar system. But unlike other unmagnetized bodies, Mars has crustal magnetic fields. These crustal magnetic fields are remnants from when the planet possessed a global magnetic fields, and they are scattered in clusters across the planet's surface. When the IMF encounters Mars' crustal magnetic fields, it produces an intricate topological system (Weber et al., 2017).

When the IMF interacts with the crustal magnetic fields, there are two outcomes based on the location of the magnetic fields: either the crustal magnetic field lines reconnect with the IMF to produce connective lines between the planet and the solar wind, or barely anything is affected, and the result is simply small-scale magnetic shields. This is why auroral emissions (due to energetic inputs from the Sun) are usually limited to localized regions of the Martian atmosphere. This in turn means that variations in magnetic topology can affect particle escape rates, which may have played a role in the planet's magnetic field evolution (Weber et al., 2017).

Magnetic fields at Mars typically have one of three topologies: closed, open, or unconnected (draped). Closed field lines are where the field lines are connected at both ends to Mars. Open field lines are where the field lines are connected to Mars at one end and to the IMF at the other. And finally, draped field lines are where the field lines are only connected to the IMF (Weber et al., 2017).

Magnetic field topologies can be identified using pitch angle distributions, which vary with local time on the nightside of Mars. Pitch angle distributions can accurately characterize the nightside environment, but dayside analysis may be a bit more complicated due to the presence of active photoelectron production. Sources of the crustal magnetic field on the nightside exhibit nearly uniform closed topology. They are usually of composed of a core which is lacking electrons, surrounded by an outer layer of mirroring particles. Whereas open field lines are found across the nightside in two favored configurations. They either drape across all regions not dominated by crustal sources, or they extend to the lowest altitudes near crustal cusps, where they descend vertically downwards (Weber et al., 2017).

The Mars Global Surveyor (MGS) was able to detect localized magnetic fields in the Southern Hemisphere of Mars. At present, the strongest measured fields were about 0.16 nT at an altitude of nearly 100 km. Considering that this field combines with the ambient ionospheric pressure, it is strong enough to deflect some of the solar wind that reaches Mars. The solar wind magnetic field lines are compressed, and they drape around the planet below the

bow shock. Remnant crustal magnetism causes the localized magnetic fields on Mars. This suggests that Mars may have once had a geodynamo with a magnetic moment that may have been larger than or equal to that of Earth's present dynamo (Lissaeur and de Pater, 2013).

The image below (figure 3.9) shows a theory of the evolution of the magnetic field lines of Mars.

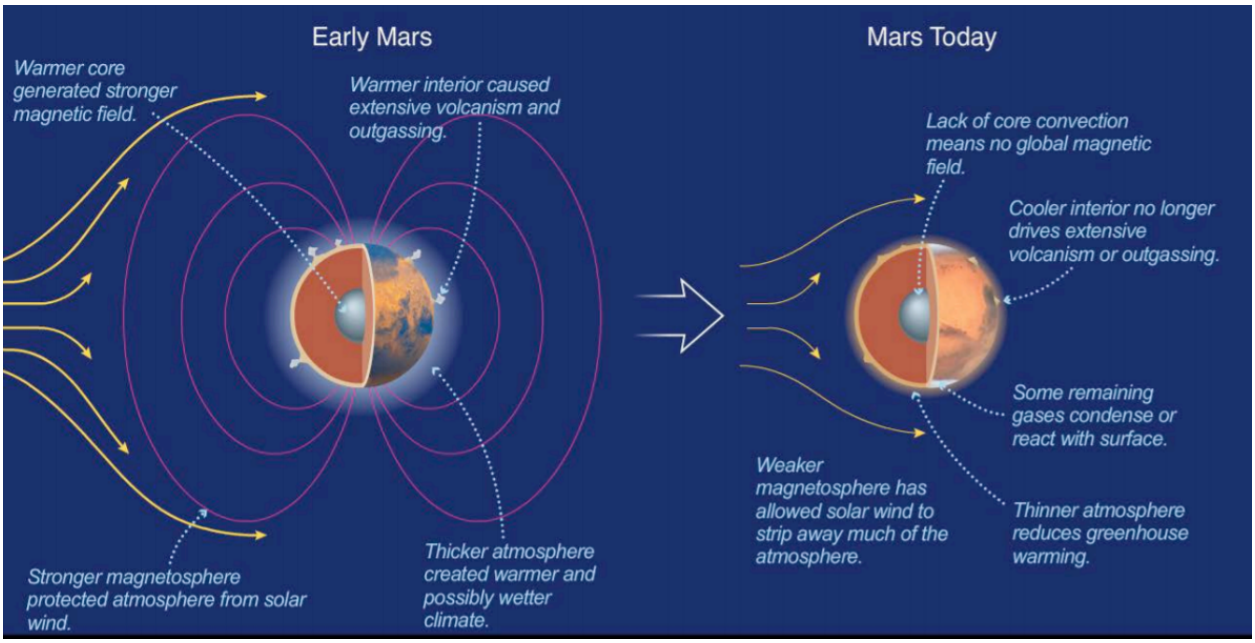

Figure 3.9. Mars of the past vs. Mars today (image is from *The Cosmic Perspective* by Bennett, 2017).

About 3 billion years ago, Mars' climate changed drastically. This climate change had a huge effect on the magnetic field and dynamo of the planet (Bennett, 2017).

3.2.4 Physical Interpretation of Special Features in Orbit 5738

I have decided to study features H and I because they are the most linear features (see figures 3.5 and 3.8). Since this aurora event was a product of the SEP event, studying the size of the intensity pixels in these features has allowed me to narrow down the kind of particle (electron or proton) and eliminate an energy range corresponding to any gyroradius that is too large compared to the upper limit that I calculated.

- A Closer Look at Feature H:

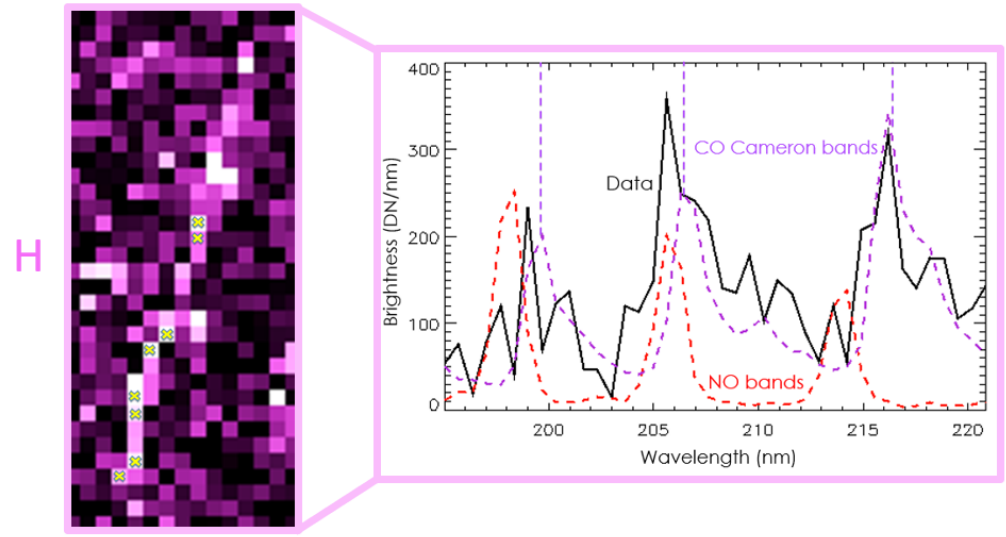

Figure 3.10. Feature H: a bright linear auroral feature.

The spectrum peaks in the exact locations as the CO Cameron bands.

- A Closer Look at Feature I

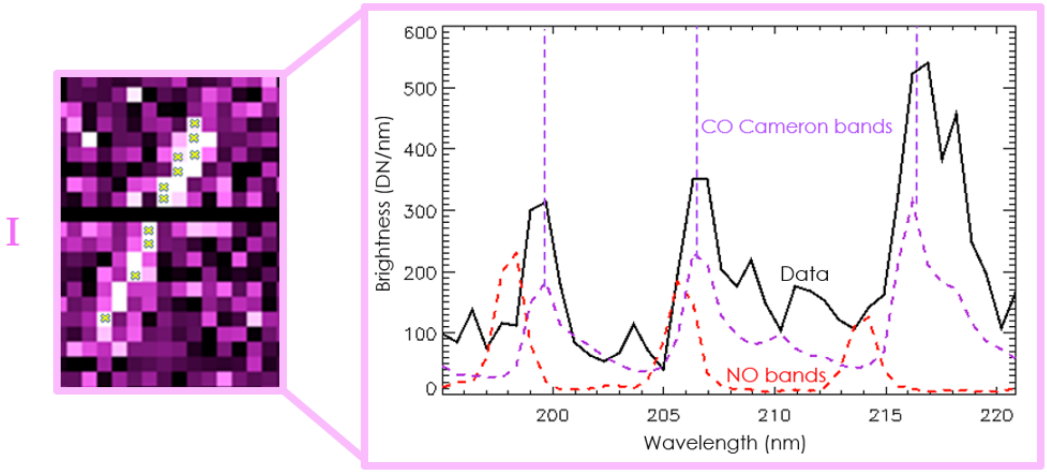

Figure 3.11. Feature I: another bright linear auroral feature.

This spectrum also peaks in the exact locations of CO Cameron bands. Feature I seems to display a geographically wider auroral feature than Feature H.

The locations of the pixels that I used to create the soectrum images for features H and I are included in Tables A.7 and A.9.

IUVS provides the data needed to determine the latitude and longitude of every corner of every pixel in the swath images (see figure A.2 in the Appendix for a sketch of what the indices on each pixel look like). I have taken this data (see Appendix Tables A.6 and A.8) and converted the longitude differences between two corners of pixels in H and I in order to determine the average width (in kilometers) of every pixel, using an IDL programming function called "MAP_2POINTS". This has allowed me to determine that on average, each pixel is about 22 km wide, in the longitudinal direction. Since there are on average 1 to 2 bright pixels lined up horizontally next to each other in both features H and I, this allows me to estimate that the bright aurora about 22–44 km. In this case, the 22 km acts as an upper limit to the gyroradius of the particles that are causing the discrete auroras to form.

3.2.5 Gyroradius Study of the Particles in Features H and I

The gyroradius (also known as the Larmor radius) of a particle is the radius of the orbit of a charged particle moving in a uniform, perpendicular magnetic field. The gyroradius is defined by the following equation:

$$r_g = \frac{mv}{|q|B} \tag{3.1}$$

The velocity in the above equation can be derived from the equation for kinetic energy:

$$E = \frac{1}{2}mv^2 \implies v = \sqrt{\frac{2E}{m}} \tag{3.2}$$

In order to narrow down what kind of particle (and its corresponding energy range) is causing the auroral features and patches in Orbit 5738, I have created the following tables and plots below that show the gyroradius of a particle with a certain energy and at a certain magnetic field. It is important to note that the tables and plots below do not give an exact answer as to what particle is causing the aurora. It simply allows me to rule out which particle it definitely cannot be.

		B (nT)		
		100	300	500
E (eV)	10^1	0.03	0.01	0.007
	10^2	0.11	0.04	0.02
	10^3	0.34	0.11	0.07
	10^4	1.07	0.36	0.21
	10^5	3.37	1.12	0.67
	10^6	10.66	3.55	2.13

(a) Electrons

		B (nT)		
		100	300	500
E (eV)	10^1	1.44	0.48	0.29
	10^2	4.57	1.52	0.91
	10^3	14.45	4.82	2.89
	10^4	45.69	15.23	9.14
	10^5	144.50	48.17	28.90
	10^6	456.94	152.31	91.39

(b) Protons

Table 3.1. Tables of the gyroradii (in km) of the two different particles.

Tables 3.1 (a) and (b) have the following distributions:

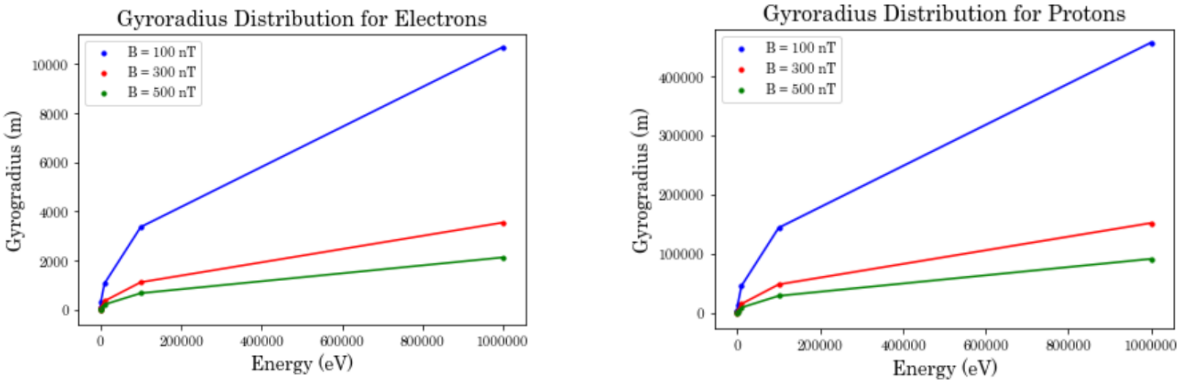

(a) Line plot of the gyroradius distribution for electrons

(b) Line plot of the gyroradius distribution for protons

Figure 3.12. Plot distributions of the gyroradii.

The plots show that the distribution is nearly identical for electrons and protons. The highest value of a gyroradius is reached at the largest energy, with the smallest magnitude of the magnetic field. However, the largest value for the gyroradius of a proton is about 40 times larger than that of an electron.

I have already determined an estimate of the gyroradius of particle based on how wide each intensity pixel is (approximately 22 km), so now I need to rule out the values in the tables that are definitely not the particles in question. See table 3.2.

		B (nT)		
		100	300	500
E (eV)	10^1	0.03	0.01	0.007
	10^2	0.11	0.04	0.02
	10^3	0.34	0.11	0.07
	10^4	1.07	0.36	0.21
	10^5	3.37	1.12	0.67
	10^6	10.66	3.55	2.13

(a) Electrons

		B (nT)		
		100	300	500
E (eV)	10^1	1.44	0.48	0.29
	10^2	4.57	1.52	0.91
	10^3	14.45	4.82	2.89
	10^4	~~45.69~~	15.23	9.14
	10^5	~~144.50~~	~~48.17~~	~~28.90~~
	10^6	~~456.94~~	~~152.31~~	~~91.39~~

(b) Protons

Table 3.2. Tables of the gyroradii (in km) with certain values crossed out.

These same tables were shown above, but there are values that were deemed too large when compared to the upper limit of 22 km, and were therefore ruled out. These values are large energies that belong to protons, and if there really were particles in the SEP event that had

these energies, the auroral features like H and I would be much more broad in the longitudinal direction. And while the 22 km acts as an upper limit for the values in these tables, I still do not have enough data in order to provide a lower limit, so the small values for the gyroradius in the tables above will not be ruled out.

3.2.6 Conclusions about Orbit 5738

Studying the localized emissions from September 14 has allowed me to confirm that the observed signal was consistent with expected auroral spectra (CO Cameron band spectra) and can be classified as discrete aurora. Projecting their locations on a map of the crustal magnetic field has confirmed the expectation that discrete aurora falls near open magnetic field lines, which is exactly as expected.

A study of the gyroradii of electrons and protons in an energy range of 10 to 10^6 eV and in a magnetic field range of 100 to 500 nT, in comparison to the pixel size of 22 km, has allowed me to conclude that the particle is either an electron, or a low-energy proton.

3.3 Study of Other Orbits

I have looked at other orbits in the event in order to see if there are patterns pertaining to the kind of emissions seen throughout the event, as well as their locations on the disk and limb of the planet.

3.3.1 Orbit 5725

Orbit 5725 was one of the very first orbits during the aurora event. It doesn't show very bright emission in the CO Cameron band end of the spectrum, but it does show quite a bit of bright NO emission along the limb of the planet. See figure 3.13.

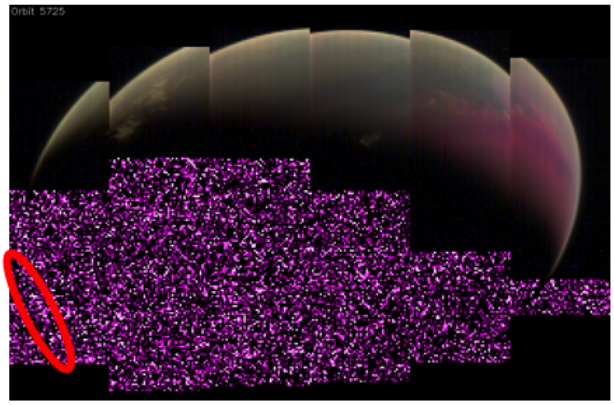

(a) CO Cameron band swath image for orbit 5725

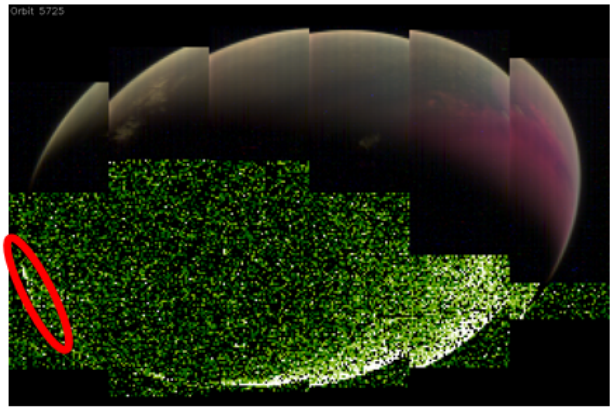

(b) NO emission swath image for orbit 5725

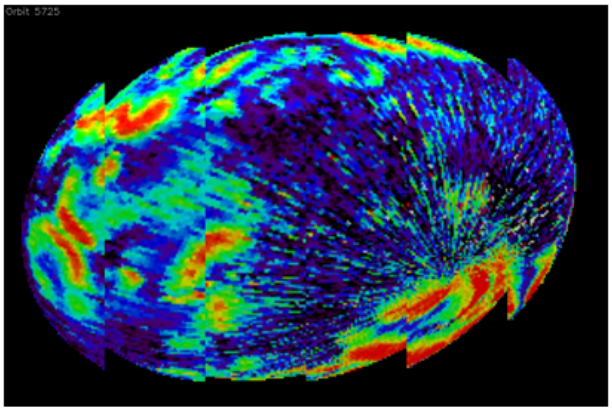

(c) Crustal magnetic field map for orbit 5725

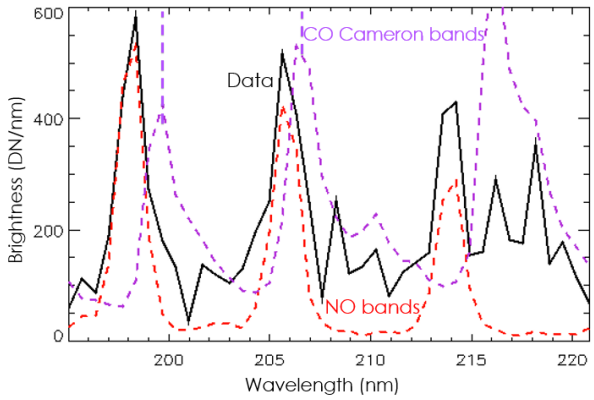

(d) Spectrum plot corresponding to the highlighted red area

Figure 3.13. Various types of data images for orbit 5725.

The highlighted red area in the CO Cameron band swath image and the NO emission swath image shows bright pixels in both images. And further investigation of the spectrum of this area shows that the bright pixels along the outline of the planet are mostly NO emissions.

3.3.2 Orbit 5730

Orbit 5730 was the one that came right before orbit 5731, which was the orbit with the brightest auroral emissions. Orbit 5730 begins to show sign of CO Cameron band emission along the disk of the planet, and there is some NO emission along the limb of the planet. See figure 3.14.

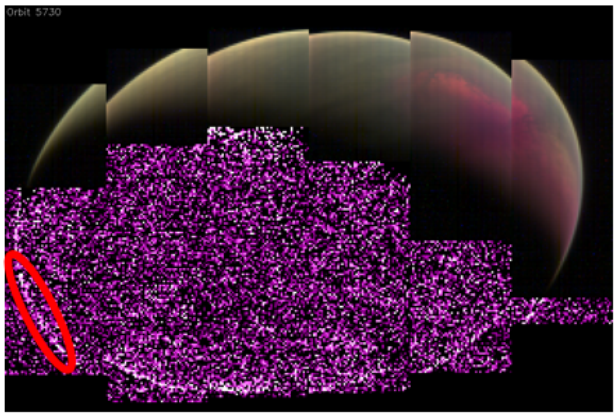

(a) CO Cameron band swath image for orbit 5730

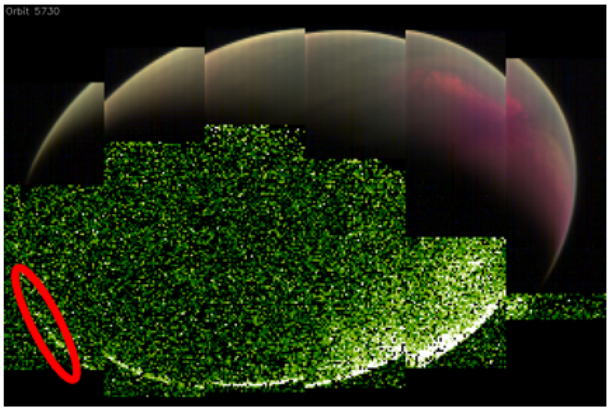

(b) NO emission swath image for orbit 5730

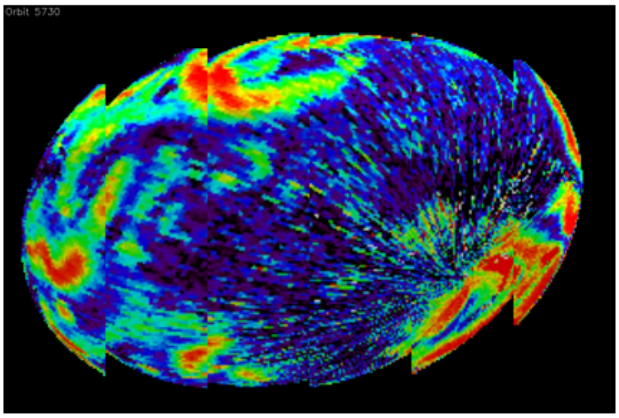

(c) Crustal magnetic field map for orbit 5730

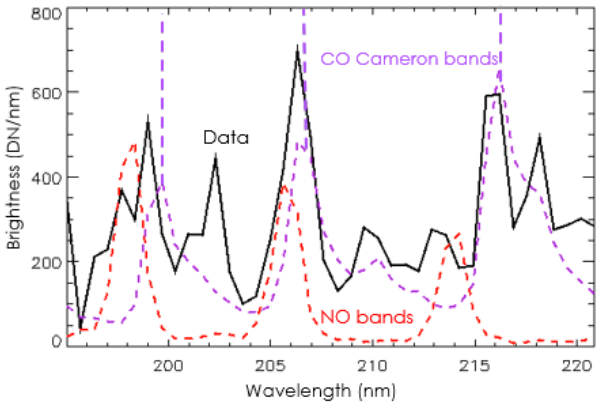

(d) Spectrum plot corresponding to the highlighted red area

Figure 3.14. Various types of data images for orbit 5730.

The highlighted red area in the CO Cameron band swath image and the NO emission swath image shows brighter pixels in the CO Cameron band swath image (see figure 3.14(a)). The spectrum of this area shows that the bright pixels along the outline of the planet, and along the disk of the planet, can be identified as CO Cameron band emissions. This matches what would be expected since this orbit is very close to the peak of the auroral event.

3.3.3 Orbit 5737

Orbit 5737 was the one directly prior to orbit 5738. Unlike Orbit 5738, this orbit lacks anomalous auroral features and patches. See figure 3.15.

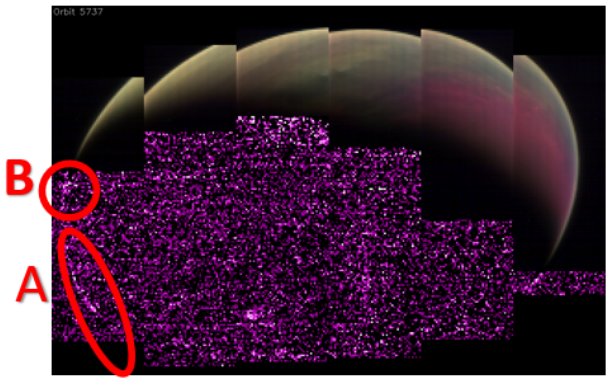

(a) CO Cameron band swath image for orbit 5737

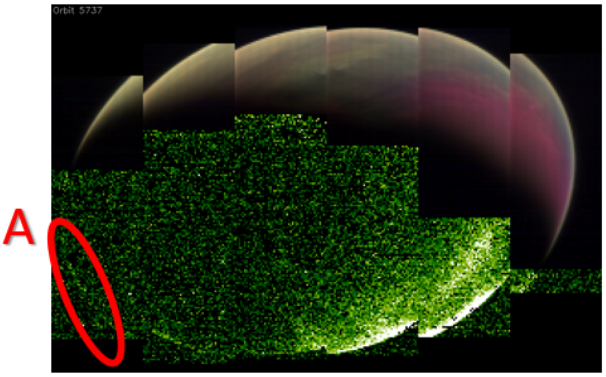

(b) NO emission swath image for orbit 5737

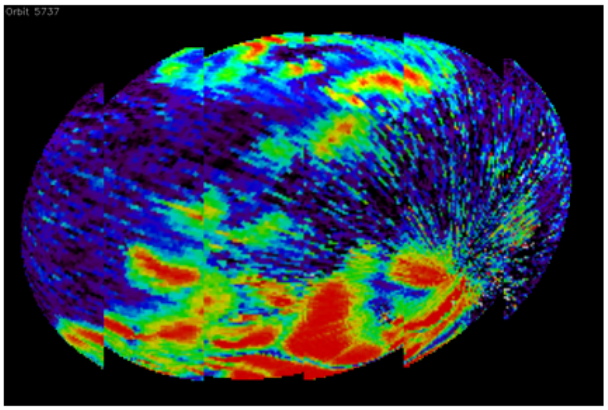

(c) Crustal magnetic field map for orbit 5737

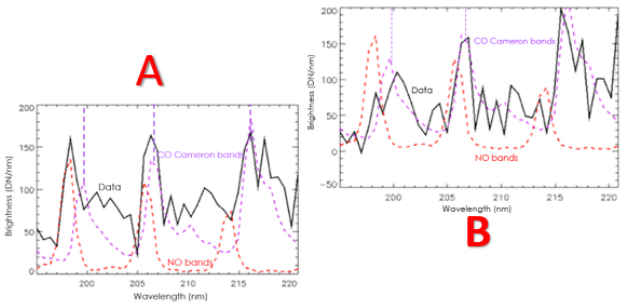

(d) Spectrum plots corresponding to the two highlighted red areas

Figure 3.15. Various types of data images for orbit 5737.

Feature A shows that areas that appear bright in both CO Cameron band and NO emission swath emissions typically indicate bright emissions in both spectra, so the data will look like a combination of both CO Cameron bands and NO. Feature B can only be seen in the CO Cameron band swath image, and studying its spectrum indicates that it is a real auroral signal.

Upon inspecting other orbits during this aurora space weather event, I was able to conclude that most of the bright pixels that we see form around the outline of the disk of the planet, and not in patches or linear features like in orbit 5738. NO emission is seen in nearly all the other orbits.

In all the orbits shown above, the bright features with data that matches the CO Cameron band template are in dark blue areas on the crustal magnetic field maps, which is exactly as expected. Once again, auroral emission that matches the discrete auroral spectra falls in areas where the crustal magnetic field lines are open.

It is important to note that the absence of the linear areas and bright patches of aurora from other orbits during this event does not mean the aurora did not occur, it simply means that

the spacecraft was not necessarily in the right geographical region or orientation to make these detections.

Chapter 4

Conclusions

The goal of this study was to understand the brightest auroral event IUVS has observed on Mars, especially during its declining phase where IUVS observed a localized aurora event in the southern hemisphere. Studying the localized emissions from September 14 has allowed me to confirm that the observed signal was consistent with expected auroral spectra and can be classified as discrete aurora. In addition, projecting their locations on a map of the crustal magnetic field has confirmed the expectation that discrete aurora falls near open magnetic field lines, or in the cusps of the crustal magnetic field of Mars.

The global aurora event displayed aurora that was 25 times brighter than anything any instrument had ever detected on Mars before. The brightest orbit was 5731, but there are others like 5738 that have special interesting features.

Other orbits in the event may not have shown any interesting features because of the spacecraft's location or orientation. Nevertheless, most other orbits showed quite a bit of NO emission.

The particles that are most likely to have caused the discrete aurora features in orbit 5738 were either electrons or protons with low energies (10 to 10^3 eV). If the particles were really electrons and not protons, there are two kinds of electrons that could be the possible source for the discrete aurora that was seen during orbit 5738: low-energy electrons accelerated by field-aligned potentials, or some high-energy electrons that are being controlled by the crustal magnetic field, and are usually responsible for diffuse aurora. Further studies need to be conducted in order to additionally narrow down an exact energy range or to eliminate one particle as the source, as well as the effect of the crustal magnetic field on energetic electrons.

Appendix: Reference Images and Data Tables

Integration	Position
99	6
101	6
101	7
107	14
110	17
111	17
119	35

Table A.1. Orbit 5731 Data Table

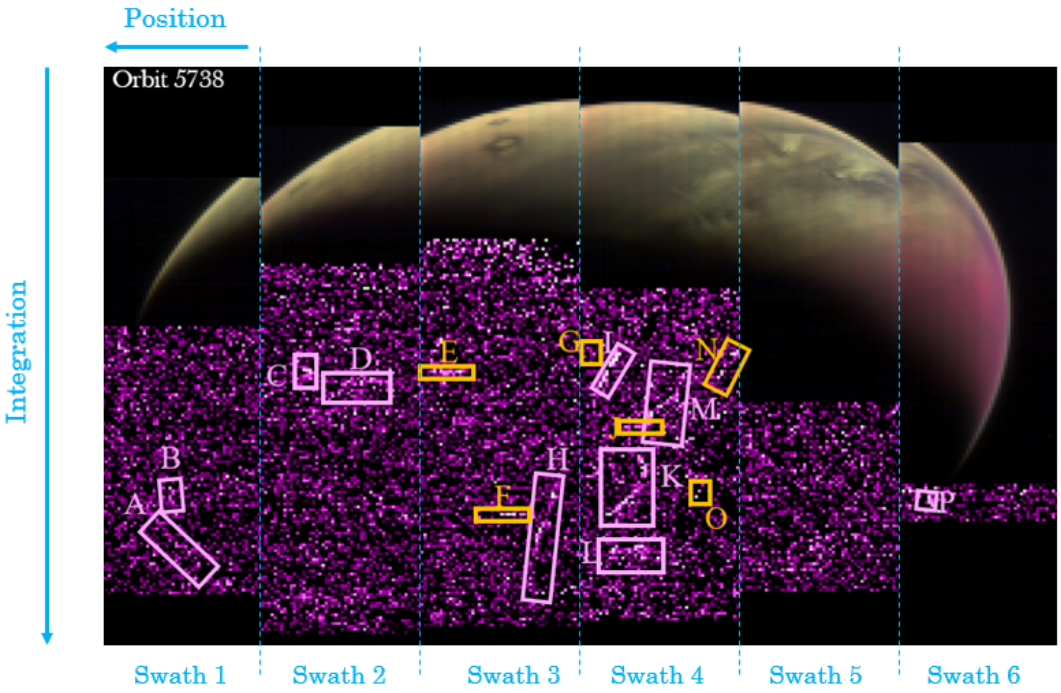

Figure A.1. A labeled swath image of Orbit 5738, simply included for reference.

Integration	Position	Integration	Position
62	35	69	30
63	34	70	29
64	33	71	29
65	33	72	28
66	32	73	28
67	32	75	26
66	30	69	30
67	30		

Table A.2. Feature A Data Table (Swath 1)

Integration	Position	Integration	Position
41	10	39	19
40	10	39	21
40	11	40	22
40	12	40	23
40	13	41	23
39	14	41	24
39	15	43	24
39	17	43	25
40	18	44	25
41	18	43	25

Table A.3. Feature D Data Table (Swath 2)

Integration	Position	Integration	Position	Integration	Position	Integration	Position
77	40	72	35	66	31	59	30
76	39	71	34	64	29	58	30
76	38	71	34	63	29	58	31
75	38	69	33	62	29	57	31
75	37	69	32	61	29	55	32
74	37	69	31	60	29	59	30
74	36	68	31	63	30	69	32
73	36	67	30	61	30		

Table A.4. Feature K Data Table (Swath 4)

Integration	Position
22	0
22	1
22	2
22	5
23	5

Table A.5. Feature N Data Table (Swath 4)

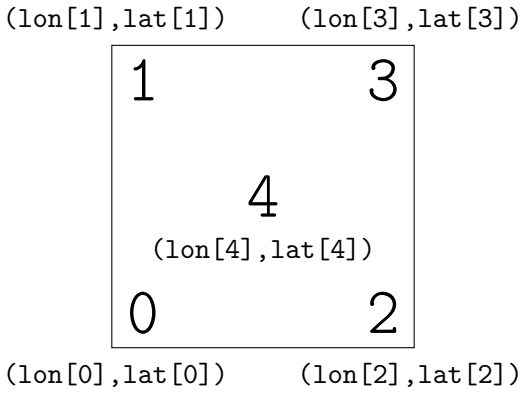

Figure A.2. Pixel Indices.

Point	Longitude	Latitude
0	159.27177	-53.027253
1	158.08510	-52.980812
2	159.47876	-52.612784
3	158.30651	-52.566782
4	158.93135	-52.815346

Table A.6. Feature H Longitude and Latitude Table (Swath 3)

Integration	Position
106	13
103	13
102	13
99	12
98	11
92	9
91	9
88	8

Table A.7. Feature H Data Table (Swath 3)

Point	Longitude	Latitude
0	208.80891	-52.171931
1	208.23293	-52.440067
2	208.53700	-51.827578
3	207.96398	-52.094315
4	208.46502	-52.110200

Table A.8. Feature I Longitude and Latitude Table (Swath 4)

Integration	Position
22	38
23	38
23	39
24	38
24	39
25	40
26	40
28	41
29	41
31	42
34	44

Table A.9. Feature I Data Table (Swath 4)

Note: I did not include data tables for orbits 5725, 5730, and 5737 because these orbits showed more peaks corresponding to NO emission, rather than CO Cameron band emission.

References

Bennett, J. O., et al. (2017). *The Cosmic Perspective*. Boston: Pearson, 291.

Bertaux, J., et al. (2005). Discovery of an aurora on Mars, *Nature, 435*. Retrieved from https://www.nature.com/articles/nature03603

Bhardwaj, A., and Jain, S. (2013). CO Cameron band and CO_2^+ UV doublet emissions in the dayglow of Venus: Role of CO in the Cameron band production. *J. Geophys. Res. Space Phys., 118*. Retrieved from https://arxiv.org/pdf/1305.6139.pdf

Brain, D. A., et al. (2006). On the origin of aurorae on Mars. *Geophysical Research Letters, 33*. Retrieved from https://agupubs.onlinelibrary.wiley.com/doi/epdf/10.1029/2005GL024782

Connour, K., et al. (2017). Three Types of Aurora Observed by MAVEN/IUVS: Implications for Mars' Upper Atmosphere Energy Budget [Abstract]. Retrieved from https://orbi.uliege.be/handle/2268/205359

Gérard, J. C., et al. (2017). The Mars diffuse aurora: A model of ultraviolet and visible emissions. *Icarus, 288*. Retrieved from http://adsabs.harvard.edu/abs/2017Icar..288..284G

Halekas, J. S. (2017). Seasonal variability of the hydrogen exosphere of Mars. *J. Geophys. Res. Planets, 122*. Retrieved from http://lasp.colorado.edu/home/maven/files/2017/05/Seasonal-variability-of-the-hydrogen-exosphere-of-Mars-1.pdf

Howell, E. (2016). Gorgeous Mars 'Nightglow' Spotted by NASA Orbiter. Retrieved from https://www.space.com/34424-mars-nightglow-nasa-maven-orbiter.html

Jakosky, B. M., et al. (2015). The Mars Atmosphere and Volatile Evolution (MAVEN) Mission. *Space Sci Rev, 195* (3). Retrieved from https://doi.org/10.1007/s11214-015-0139-x

Kramer, M. (2017). MAVEN: NASA's Orbiter Mission to Mars – Mission Details. Retrieved from https://www.space.com/23617-nasa-maven-mars-mission.html

LASP. (2018). Exploring Mars' Climate History. Retrieved from http://lasp.colorado.edu/home/maven/

LeBlanc, F., et al. (2006). Origins of the Martian aurora observed by Spectroscopy for Investigation of Characteristics of the Atmosphere of Mars (SPICAM) on board Mars Express. *J. Geophys. Res., 111.* Retrieved from https://agupubs.onlinelibrary.wiley.com/doi/full/10.1029/2006JA011763

Lissaeur, J. J., and de Pater, I. (2013).Fundamental Planetary Science. *Cambridge University Press*, 253-255.

McClintock, W. E., et al. (2015). The Imaging Ultraviolet Spectrograph (IUVS) for the MAVEN Mission. *Space Sci Rev, 195: 1–4.* Retrieved from https://link.springer.com/article/10.1007/s11214-014-0098-7

NASA. (2017). Large Solar Storm Sparks Global Aurora and Doubles Radiation Levels on the Martian Surface. Retrieved from https://www.nasa.gov/feature/jpl/large-solar-storm-sparks-glo

Ritter, B., et al. (2018a). Aurorae on Mars, Scientific Workshop: "From Mars Express to ExoMars" [Abstract]. Retrieved from https://www.cosmos.esa.int/documents/1499429/1583871/Ritter_B.pdf

Ritter, B., et al. (2018b). Observations of the proton aurora on Mars with SPICAM on board Mars Express. *Geophys. Res. Lett., 45.* Retrieved from https://agupubs.onlinelibrary.wiley.com/doi/abs/10.1002/2017GL076235

Schneider, N. M., et al. (2015). Discovery of Diffuse Aurora on Mars. *Science, 350.* Retrieved from https://pdfs.semanticscholar.org/d71a/951e3571ea97ad5b587bac50892a8660ce62.pdf

Schneider, N. M., et al. (2018). Global aurora on Mars during the September 2017 Space Weather Event. *European Geosciences Union, 20.* Retrieved from https://meetingorganizer.copernicus.org/EGU2018/EGU2018-3546.pdf

Stiepen, A., et al. (2015). Mars thermospheric scale height: CO Cameron and CO_2^+ dayglow observations from Mars Express. *Icarus, 245.* http://planetary.aeronomie.be/multimedia/pdf/Stiepen_15a.pdf

Weisstein, E. W., et al. (2007). Homopause. Retrieved from http://scienceworld.wolfram.com/astronomy/Homopause.html

Acknowledgements

I would like to express the utmost gratitude for everyone who has helped me make it this far in my educational career:

- Dr. Nick Schneider, Dr. Derek Brown, Dr. Dave Brain, Dr. Ann-Marie Madigan, and Dr. Fran Bagenal who inspired me to love this field of science as much as they do.
- My professors who pushed me to work harder and allowed me to realize how amazing this world of science truly is.
- My parents and sisters who supported me and helped me get up when I was down.
- My best friends who were there for me and believed in me.
- The MAVEN/IUVS team for providing me with all the data and help that I needed.

Thank you all very much.